Spatial coherency analysis of seismic ground motions from a rock site dense array implemented during the Kefalonia 2014 aftershock sequence

Angkeara Svay, Vincent Perron, Afifa Imtiaz, Zentner Irmela, Régis Cottereau, Didier Clouteau, Pierre Yves Bard, F. Hollender, Fernando Lopez-Caballero

Spatial coherency analysis of seismic ground motions from a rock site dense array implemented during the Kefalonia 2014 aftershock sequence

A. Svay[1,2,3,*,†], V. Perron[4,5], A. Imtiaz[5], I. Zentner[2,3], R. Cottereau[1], D. Clouteau[1], P.-Y. Bard[5], F. Hollender[4,5] and F. Lopez-Caballero[1]

[1]*Laboratory of Mechanics of Soils, Structures and Materials, CNRS, UMR8579, CentraleSupélec, Université Paris-Saclay, Châtenay-Malabry, France*
[2]*Institute of Mechanical Sciences and Industrial Applications, UMR 9219 EDF-CNRS-CEA-ENSTA ParisTech, Université Paris Saclay, Palaiseau, France*
[3]*EDF Lab Paris-Saclay, Palaiseau, France*
[4]*French Alternative Energies and Atomic Energy Commission (CEA), Saint-Paul-les-Durance, France*
[5]*Institut des Sciences de la Terre, French Institute of Science and Technology for Transport, Development and Networks, University Grenoble-Alpes, Grenoble, France*

The objective of studies presented in this paper is to analyse the spatial incoherency of seismic ground motions using signals from a velocimeter dense array located on a rock site, recording the aftershock sequence of the two M6 Kefalonia earthquakes that occurred in January/February 2014 (Kefalonia island, Greece). The analyses are carried out with both horizontal and vertical components of velocigrams for small separation distances of stations ($<$100 m). The coherencies of seismic ground motions identified from strong motion windows are compared with those identified from coda parts of signals. It is realized that there is no significant difference between the coherencies estimated from those two parts of signals. The influence of earthquake event number on the result of coherencies and the dispersions of coherencies estimated from different earthquake events are presented. Finally, coherencies estimated from the dense array are compared with several coherency models proposed and widely used in the literature. The possibility of modifying some parameters of those existing coherency models to fit with *in situ* coherencies are discussed and presented.

KEY WORDS: spatial variability; ground motion dense array; coherency model; soil–structure interactions

1. INTRODUCTION

In seismic soil–structure interaction analyses, a common practice in Civil Engineering is to consider a uniform motion of free field at any point on the ground surface. However, that assumption is not completely realistic [1, 2] because the seismic ground motions can vary spatially due to many different factors such as slip distribution, source-to-site distance, travel path geology, attenuation, scattering of seismic wave propagations, site geology, and site topography [3].

*Correspondence to: Angkeara Svay, CentraleSupélec & EDF Lab Paris-Saclay Palaiseau, France.
†E-mail: angkeara.svay@centralesupelec.fr

For a given site, the term 'spatial variability' refers to the differences in terms of amplitude and phase of seismic motions at two observation points at a given time. Among different factors listed earlier, three principal factors that create spatial variations of seismic ground motions are as follows [1, 2] :

1) Wave passage effects: refers to the difference in the arrival times of waves at separate stations. One can generally recognize this factor for the inclined incident plane waves. The wave passage time delay between two locations will introduce a shift in the Fourier phases of the earthquake ground motions.
2) Site effects: refers to the difference in local site conditions at each station that can be site geology and site topography (e.g. sedimentary valleys). This term can alter the amplitude and frequency content of the bedrock motions differently. For the sedimentary valleys, the seismic waves get trapped within the valley, and surface waves develop at the basin edge leading to large amplification on the sediment sites compared with the rock site.
3) Effect of 'pure incoherence': refers to the result of the refraction and the reflection of seismic wave (wave scattering) that occurs as waves propagate in a heterogeneous medium and also, the superposition of waves arriving from different parts of an extended site.

Many studies, reported in the literature, show the effects of the spatial variability of seismic excitations on the structural responses for both extended structures [4–10] and multi-supported structures [11–14]. For the favourable effects, one can observe the filtering of movements of translation at high frequencies. The introduction of the spatial variability of seismic excitations can then lead to reduce the structural response-spectra [5, 8], but the spatial variation of seismic ground motion can also generate additional forces known as pseudo-static forces, which are absent when the structure is subjected to a uniform support motion [12, 15].

The spatial incoherence of seismic ground motions due to dispersions and reflections of seismic waves (*pure incoherence*) can be modelled 'in a probabilistic frame work' by a coherency function. The 'coherency function' is a normalized function obtained by the ratio between the smoothed-crossed spectral density (cross spectrum S_{jk}) and the smoothed-power spectral densities (power spectra: S_{jj} and S_{kk}) of two observed accelerograms at j and k station points:

$$\gamma(d_{jk}, \omega) = \frac{\overline{S}^{M}_{jk}(\omega)}{\sqrt{\overline{S}^{M}_{jj}(\omega) \cdot \overline{S}^{M}_{kk}(\omega)}} \tag{1}$$

where d_{jk} is the distance between j and k, ω is the circular frequency and over-line with M represent the smoothing of power spectra (the description of these smoothing spectra will be given in detailed in the Section 3.1.1, Equation (3)).

Several models of coherency function were proposed in the literature to represent the spatial variability of seismic ground motions in the analyses of seismic soil–structure interactions. These coherency functions were applied in the soil–structure interaction analysis of extended structures or multi-support structures such as dams [16], bridges [13], pipelines [17] and also nuclear power plants [5–8]. Nevertheless, the applications of those models are still limited because some of them are purely empirical and do not have a proper relation to the physical properties of sites. This might be somewhat risky to apply these coherency models to arbitrary sites in soil–structure interaction applications as they may provide unsatisfactory estimations of the actual site-specific coherency values. For the semi-empirical functions, although their expressions are formed by theoretical considerations with parameters that can be determined from the earthquake data, a recent study of [18] shows their limitations by comparing the model with the coherencies estimated from US Geological Survey Parkfield Dense Seismograph Array [UPSAR].

The objective of studies presented in this paper is to analyse the coherency of seismic ground motions from the database of Argostoli rock-site dense array (earthquake aftershock sequence recorded in February and March 2014 in Kefalonia island, Greece) [19, 20] and to compare that coherency

with some existing coherency models. The analyses begin with the estimations of coherencies from both horizontal and vertical components of velocigrams for different separations of stations from 10 to 100 m. The difference between coherencies of strong motion windows and coda windows is also discussed. The influences of strong motion durations and earthquake event numbers on the average of plane-wave coherencies will also be analysed. Coherencies estimated from that array are finally compared with the coherency models proposed and widely used in the literature to discuss on the limitations of those existing models.

This paper is organized as the following: Section 2 describes briefly about the earthquake sequence happening at Kefalonia island in 2014, about the dense array installed at the Argostoli site for recording the ground motion signals and about the seismic signal database. After that, Section 3 reviews several existing coherency models, proposed in the literature. Different types of coherency and methodologies used for estimating them from seismic signal database are also presented. The next section, Section 4, presents the main results of statistical analyses of spatial coherency of earthquake ground motions from Argostoli database. Finally, to discuss on the limitations of some existing coherency models, the *in situ* coherencies estimated from Argostoli database are compared to those coherency models. That comparison is illustrated in the Section 5. The possibility of modifying some parameters of those models to fit them to the *in situ* coherencies are also discussed.

2. DESCRIPTIONS OF ARGOSTOLI EARTHQUAKES AND ROCK SITE DENSE ARRAY

The island of Kefalonia, located in Ionian Sea, Greece, (Figure 1) is one of the most seismically active regions in the Euro-Mediterranean area, especially because of the proximity of the Kefalonia Transform Fault that plays a major role for the transition zone between the African sub-ducting plate and the continental Apulian plate. Numerous earthquakes shook the area in the past (e.g. the major 1953, Mw 7.2 earthquake and induced an upfilt up to meter of a great part of the Kefalonia island). Because of this high seismicity, as well as the presence of sedimentary basin, the area was chosen as a test site within the framework of the French Research Agency (ANR) PIA Sinaps@ project (www.institut-seism.fr/projets/sinaps/) [22] to validate 3D non-linear computational codes through the installation of a permanent accelerometric vertical network within the basin (Koutavos area). The area benefits from a first geophysical survey conducted in September 2013 that allowed identifying and characterizing rock outcropping area, among other objectives.

Then, the Kefalonia island was shaken by two significant earthquakes on 26 January 2014 at 13:55:43 UTC ($Mw = 6.1$) and on 3 February 2014 at 03:08:45 UTC ($Mw = 6.0$) [19, 20]. This sequence motivated the organisation of a post-seismic survey [23] that aimed to deploy on the site: (i) temporary accelerometer network (waiting the installation of the Sinaps@ project permanent accelerometric network), (ii) a rotation sensor and (iii) a dense array located on the previously identified rock site (to be complementary to other previous datasets from soil sites). This paper is focused on the analysis of this last instrumentation.

The Argostoli rock-site dense array consists of 21 sensors, distributed 5 by 5 on 4 circles with respective radius of 10, 30, 90 and 180 m, plus a central station (Figure 2). This geometry leads to a star with 5 branches (corresponding to 5 equally spaced azimuths) with four stations on each branch. Each station is identified by the ID of the branch and the ID of the radius (e.g. station B2R3 means branch number 2 and radius number 3, B0R0 being the central station). All sensors were Guralp CMG6TD broadband seismometers with built-in digitizers that present a flat frequency response between 0.03 and 100 Hz. A 200-Hz sampling frequency is used for our measurements. This choice implies a good instrumental sensitivity that allows obtaining a good signal-to-noise ratio for low frequencies but also induced saturation for strongest motions.

The stations were in operation and recorded in continuous mode from 6 February 2014 to 10 March 2014. By the use of seismicity catalogues, we extracted up approximately 2000 well recorded events from this continuous databank, with local magnitudes between 1 and 5. From this whole database, 93 events were selected to process the statistical analysis on the estimation of the spatial coherency of earthquake ground motions. These 93 events are characterized by local magnitudes between 2.7 and 3.6 according to the NOA (National Observatory of Athens) catalogue. They present focal distances

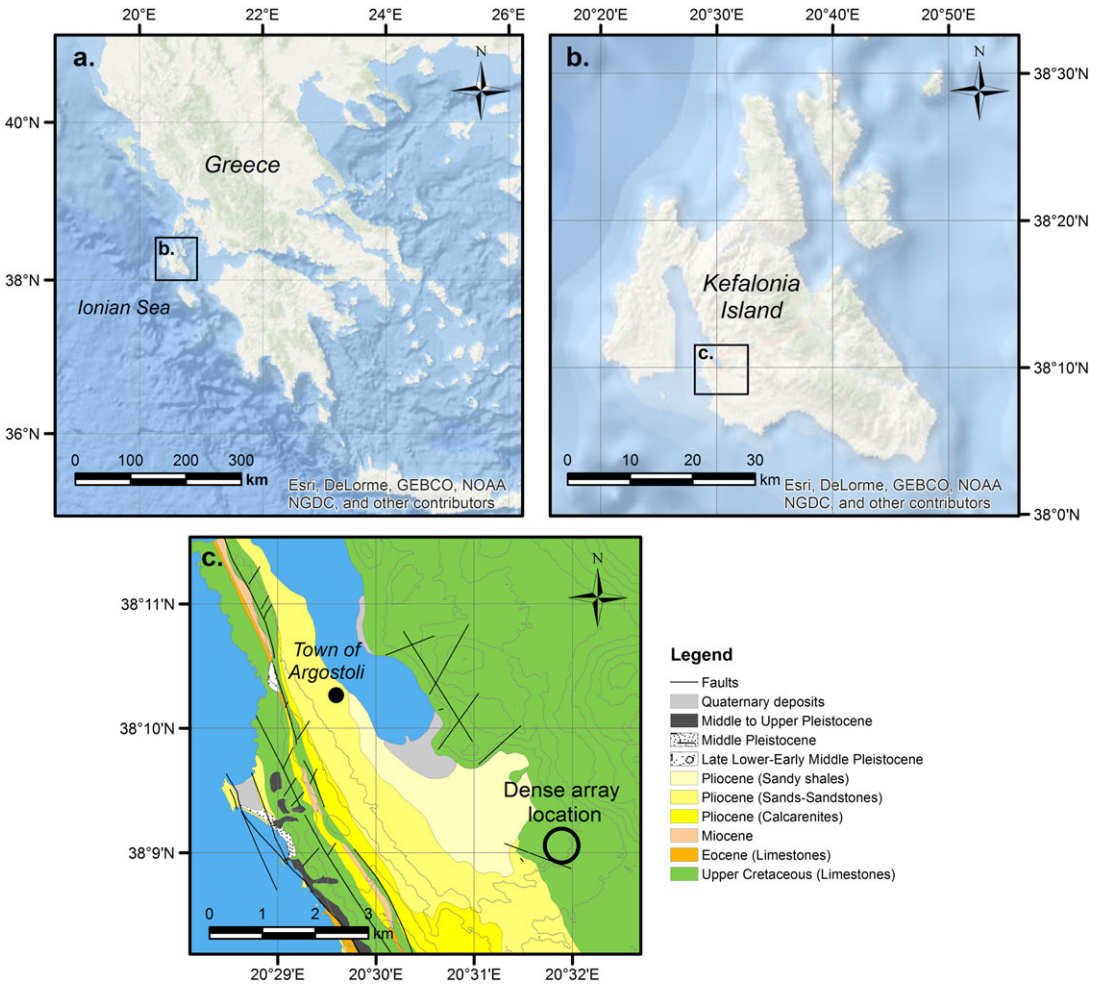

Figure 1. Location of studied site. (a) Location of Kefalonia island with respect to Greece. (b) Location of the Argostoli area with respect to Kefalonia island. (c) Location of the Argostoli rock site dense array on the local geological map [21]. [Colour figure can be viewed at wileyonlinelibrary.com]

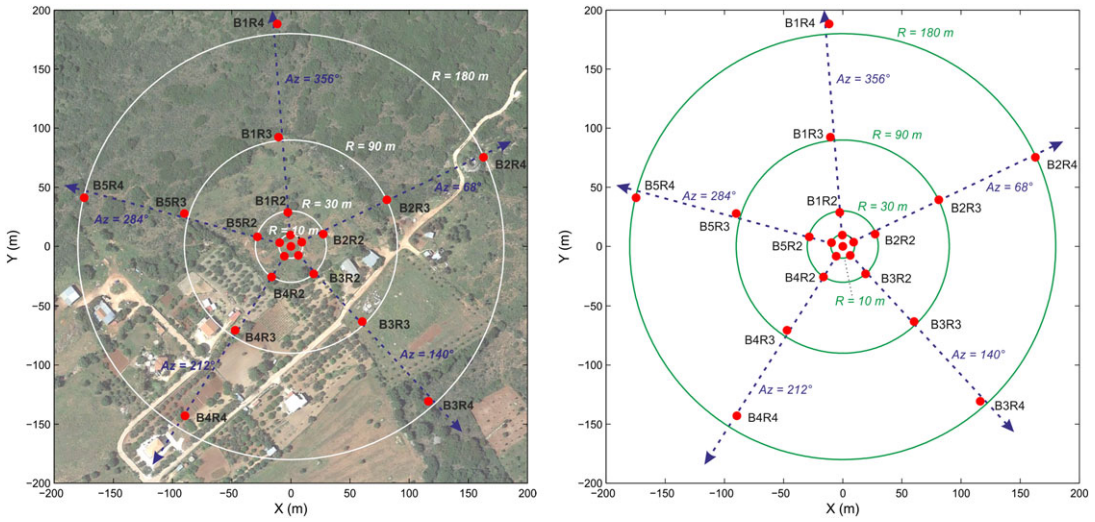

Figure 2. Argostoli rock site dense array geometry mapped on aerial photography (source : Google Earth). Each red dot represents one sensor. [Colour figure can be viewed at wileyonlinelibrary.com]

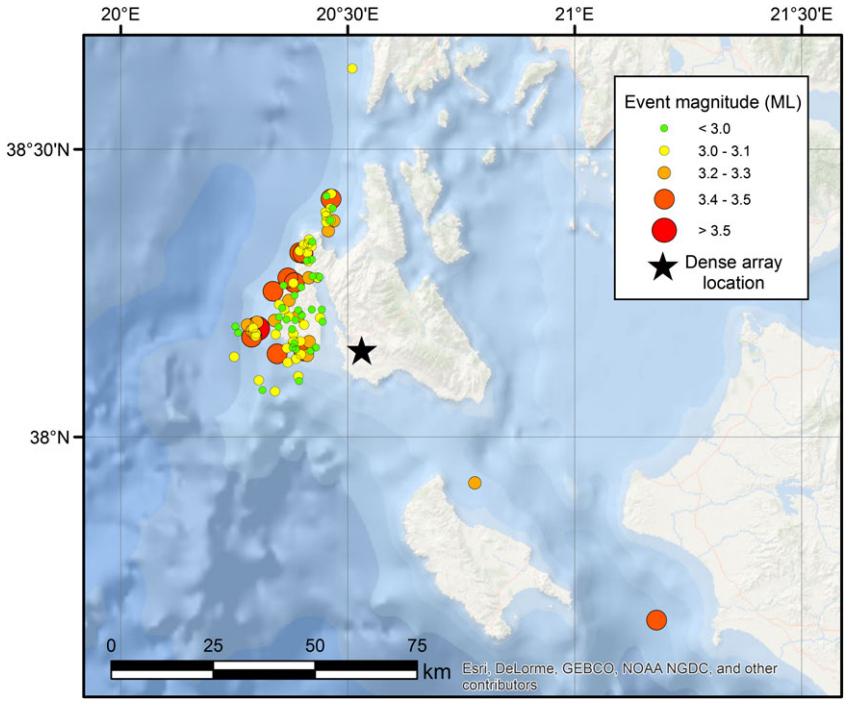

Figure 3. Epicenters of aftershocks recorded by the Argostoli rock-site dense array and used in the present study (selection of 93 earthquakes out of approximately 2000 well recorded events from 6 February 2014 to 10 March 2014). Colors indicate magnitude values. The black star represents the location of array. [Colour figure can be viewed at wileyonlinelibrary.com]

between 9 and 77 km as well as peak ground velocity from 0.05 to 2.4 mm/s. Figure 3 presents the map of the selected events. The distributions of the used events in terms of focal distance, magnitude and peak ground velocity are presented in Figure 4.

The smaller earthquakes were not used in these studies because that was desired to investigate the coherencies with motions as high as possible. Conversely, higher magnitudes induced saturation of sensors and were then not usable for coherency analysis. An example of five velocigrams along the branch B1 (Central station, B1R1, B1R2, B1R3, B1R4) for all the three directions for an earthquake event (event 2014-02-06-185141, $Mw = 3.0$, epicentral distance $= 17.4$ km) is presented in Figure 5.

As described previously, the Argostoli rock-site dense array area took benefit from a previous geophysical survey that allowed determining velocity profiles beneath the site. This geophysical survey consisted in the implementation of methods based on the analysis of surface-wave dispersion [24]. The circular passive arrays of seismometers are deployed successively to record ambient vibration. These circles had radius from 5 to 700 m. Using the spatial autocorrelation method, the analysis of these data allowed determining the dispersion curve of the fundamental mode of Rayleigh waves, which was then converted in velocity profile by inversion. Because the inversion process does not lead to unique solution, a set of possible velocity profile is showed in Figure 6. These profiles lead to Vs30 value (shear-wave velocity for the top 30 m) of about 830 ± 35 m/s.

3. REVIEWS OF SOME COHERENCY MODELS AND METHODOLOGIES FOR ESTIMATING COHERENCY FROM GIVEN SEISMIC SIGNALS

This section reviews different types of coherencies of seismic ground motions that can be used in engineering practices presented in the literature. The methodologies to estimate those coherencies are briefly presented in this section. After that, several semi-empirical and empirical coherency models proposed and widely used in the literature are presented. The expression ‘empirical functions’ refers to the functions given directly by using statistical analyses of recorded data without using any

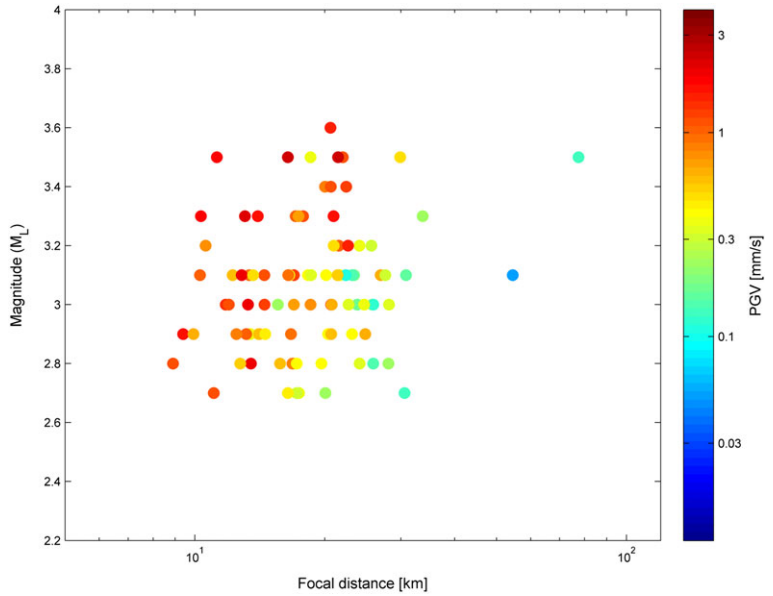

Figure 4. Distribution of selected earthquake in terms of epicentral distances (*x*-axis), magnitudes (*y*-axis) and peak ground velocity (color scale). [Colour figure can be viewed at wileyonlinelibrary.com]

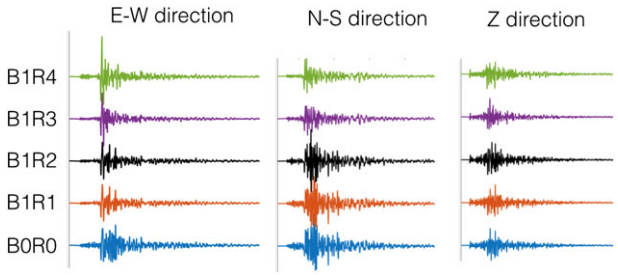

Figure 5. Velocities captured at Argostoli dense array (event 2014-02-06-185141, $Mw = 3.0$, Epicentral distance = 17.4 km). [Colour figure can be viewed at wileyonlinelibrary.com]

physical theories. 'Semi-empirical functions' refer to the functions that are formed on the basis of analytical considerations but include some parameters that require estimation from recorded data at earthquake sites. For more detailed reviews of coherency function models, the reader is referred to the analyses of [25].

3.1. Types of coherencies and methodologies for estimating coherencies

There are several types of coherencies that can be derived from earthquake signals: complex coherency ($\gamma(d_{jk},\omega)$), lagged coherency ($|\gamma(d_{jk},\omega)|$), unlagged coherency ($\gamma^{U}(d_{jk},\omega)$) and plane-wave coherency($\gamma^{PW}(d_{jk},\omega)$) .

3.1.1. Complex coherency. As described in Equation (1), the complex coherency ($\gamma(d_{jk},\omega)$) can be estimated from the ratio between smoothed cross spectral density ($\overline{S}_{jk}^{M}$) and smoothed power spectral densities ($\overline{S}_{j}^{M}$ and $\overline{S}_{k}^{M}$). By using spectral densities to estimate the coherencies of earthquake ground motions, the hypothesis of stationary process is considered, but the earthquake ground motion signals are not stationary. Hence, only the strong motion windows of signals are used for the estimations of spatial coherencies because it is assumed that the signals are stationary in strong

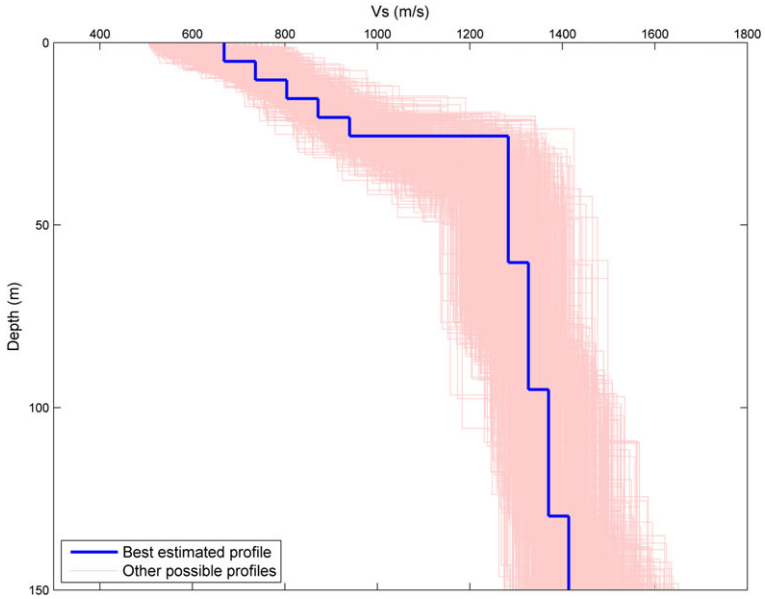

Figure 6. Shear wave velocity profiles estimated beneath the Argostoli rock site dense array. These profiles are computed using surface-wave based methods. In blue, 'best estimated' profile; in red, other possible profiles). [Colour figure can be viewed at wileyonlinelibrary.com]

motion windows. The strong motion window can be obtained by using Arias intensity (AI) that represents the energy of earthquake signals. That Arias intensity is evaluated following the expression used by Abrahamson [26]:

$$AI(\tau) = \frac{\int_{T_p}^{\tau}(V_1^2(t) + V_2^2(t))dt}{\int_{T_p}^{T_p+25}(V_1^2(t) + V_2^2(t))dt} \tag{2}$$

where T_p is the arrival time of P-wave, that is, the beginning of earthquake signals, and $V_1(t)$ and $V_2(t)$ are the signal velocigrams in both horizontal components. The beginning and the end of the strong motion window is considered to be at the moments when Arias Intensity reaches a value of 0.1 and 0.9. An example of the strong motion window for an earthquake event is presented in Figure 7. The red color part of the signal represents the strong motion window used for evaluating the coherency of seismic ground motions. The cosine tapering is applied to each strong motion window to obtain strong motion windows that start and end at zero amplitude.

The smoothed power spectral densities ($\overline{S}_j^M$ and $\overline{S}_k^M$) and smoothed cross spectral density ($\overline{S}_{jk}^M$) are then identified from those strong motion windows of signals. For two time series $u_j(t)$ and $u_k(t)$ (strong motion windows of earthquake ground motion signals recorded at j and k), the smoothed cross spectral density is defined by

$$\overline{S}_{jk}^M(\omega) = \sum_{-M}^{M} a_m U_j(\omega_m) U_k^*(\omega_m) \tag{3}$$

where a_m is the weights of Hamming window function used in the frequency smoothing, and $U_j(\omega)$ is the Fourier transform of $u_j(t)$ and $U_k^*(\omega)$ is the conjugate of Fourier transform of $u_k(t)$.

An 11-point Hamming window function was recommended by Abrahamson [27] for smoothing in frequency domain for time windows with less than approximately 2000 samples, if the coherency estimates were to be used for the analyses of structures with 5% critical damping. This 11-point Hamming window function is hence used in this study.

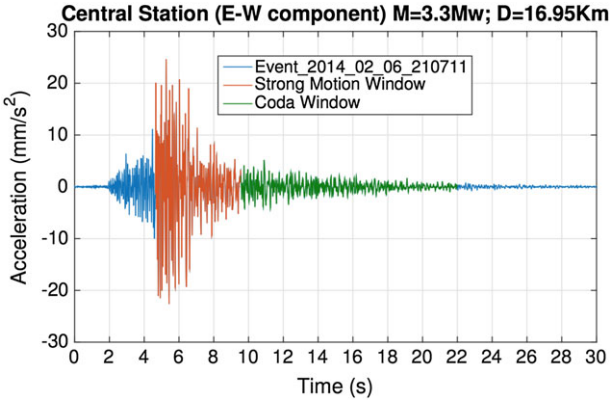

Figure 7. Strong motion window used for estimating coherency of earthquake ground motions. [Colour figure can be viewed at wileyonlinelibrary.com]

3.1.2. Lagged coherency. The complex coherency (Equation 1) has an amplitude and a phase for each frequency band. The lagged coherency is simply the modulus term (amplitude) of the complex coherency defined by

$$|\gamma(d_{jk},\omega)| = \left| \frac{\overline{S}^{M}_{jk}(\omega)}{\sqrt{\overline{S}^{M}_{jj}(\omega)\cdot\overline{S}^{M}_{kk}(\omega)}} \right| \tag{4}$$

The lagged coherency is a measure of 'similarity' in the seismic motions and indicates the degree to which the data recorded at the two stations are related. The lagged coherency reflects, at each frequency, the correlation of the motions. It is expected that at low frequencies and short separation distances, the motions will be similar and therefore, theoretically, the lagged coherency will tend to unity as frequency and station separation distance tend to zero. On the other hand, for uncorrelated processes, lagged coherency becomes zero. Hence, at high frequencies and long station separation distances, whose motions become uncorrelated, the lagged coherency will become zero [3]. However, in the estimation of lagged coherency from given seismic ground motion signals, the lagged coherency does not go to zero at large separations and high frequencies because of two possible reasons. The first one is devoted to statistical reason: the bias in the estimate of the lagged coherency [3]. The second reason is dedicated to a physical one. After Abrahamson [27], a segment of earthquake signals can contain wave components in addition to the plane wave. One's more, at high frequencies, the scattered energy or noise contribute significantly to the records. The correlation of these additional wave components will be reflected in the lagged coherency and will not let estimated lagged coherency approach zero at high frequencies and large separations.

3.1.3. Unlagged coherency. The unlagged coherency $\gamma^{U}(d_{jk},\omega)$ measures the coherency assuming no time lag between locations [27]. This corresponds *only* to the assumption of vertical wave propagation for which there is no wave passage effects on the spatial variability of seismic ground motions. The unlagged coherency is given by the real part of the complex coherency.

The coherent part of the wave passage effect can lead to negative value of the unlagged coherency. Negative values indicate that the ground motions at the two stations are out of phase. An unlagged coherency of -1 indicates that the ground motion is 180° out of phase due to wave passage effects [5].

3.1.4. Plane wave coherency. As described in Section 3.1.2, after Abrahamson [27], the lagged coherency cannot approach zero at high frequencies and large separations of stations because of the presence of some wave components (in the analysed segments of earthquake signals) in addition to the plane wave. Another point is that the lagged coherency describes only the deviations of the ground motions from plane wave propagation at *each* frequency but does not consider the deviation

of the motions from a single plane wave at *all* frequency. Accurately, the lagged coherency allows for different frequencies to have their own wave speed and direction of wave propagations. Because soil–structure interaction applications always consider a single plane wave speed and single direction at *all* frequencies, the lagged coherency is not consistent with these applications [27, 28].

Therefore, Abrahamson [27] is interested in another type of coherency called 'plane-wave coherency' $\gamma^{PW}(d_{jk}, \omega)$ that measures the coherency relative only to a single plane wave velocity for each earthquake. The plane-wave coherency can be estimated from the time histories by taking the real part of the cross-spectrum after aligning the ground motions based on the best plane-wave velocity:

$$\gamma^{PW}(d_{jk}, \omega) = \Re \left[\frac{\overline{S}^{M}_{jk}(\omega)}{\sqrt{\overline{S}^{M}_{jj}(\omega) \cdot \overline{S}^{M}_{kk}(\omega)}} \right]_{plane\_wave\_direction} \tag{5}$$

To estimate this plane wave coherency, we need to

(1) evaluate the direction of plane wave propagation
(2) rotate the signals into the direction of plane wave propagation evaluated in ()
(3) align the signals for each station pair in the direction of plane wave propagation to remove the wave passage effects and to evaluate the best-fit plane wave speed by using seismic interferometry methodology
(4) estimate the smoothed cross-spectral density, the smoothed power spectral densities and finally, the coherencies (Equation 5)

The direction of plane-wave propagations can be found from the earthquake ground motion signals by determining an angle ϕ for which the correlation coefficient between the two horizontal components (after being rotated by angle ϕ) is equal to zero. It is considered that third principal component is the vertical direction.

The coefficient of correlation between the two horizontal components (a_1 and a_2) of earthquake signals is given by [29]:

$$\rho_{1,2} = \frac{\int_0^\tau a_1(t) a_2(t) dt}{\sqrt{\int_0^\tau a_1^2(t) \int_0^\tau a_2^2(t)}} \tag{6}$$

where τ here indicates the end of signals.

After evaluating the angle ϕ for each earthquake event, a new database of signals is created by rotating all the horizontal component signals of each event by an angle ϕ of that event. Therefore, in that new database, the two signals of horizontal component are the one in first principal component (direction corresponding to angle ϕ) and another one in second principal component (direction perpendicular to angle ϕ). After rotating horizontal components into principal components, the best-fit plane-wave velocity c can be evaluated by using seismic interferometry. Accurately, for each earthquake event, by taking the central station as the referent, the signals of other stations are shifted in time by an amount of τ_o. The value of τ_o changes from station to another station depending on the distance between that station and the central station. It can be identified from the cross correlation function of signals at the central station and another station. The value of τ_o is simply the moment when the cross correlation between the two signals is maximum. After knowing τ_o, the best-fit plane wave velocity is simply the ratio between the station separations and that shifted time τ_o.

Because the real part of the smoothed cross-spectrum will have both positive and negative values, the plane-wave coherency will approach zero at high frequencies and large separation distances. The values of plane-wave coherency are less than or equal to the lagged coherency.

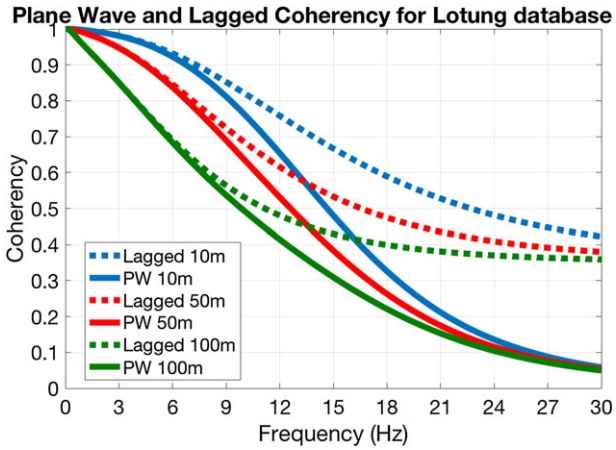

Figure 8. Comparison between plane-wave coherency and lagged coherency of Abrahamson model [27] estimated from Lotung database. [Colour figure can be viewed at wileyonlinelibrary.com]

By knowing the unlagged coherency (Section 3.1.3), the plane wave coherency can also be defined by

$$\gamma^{PW}(d_{jk}, d^r_{jk}, \omega) = \frac{\gamma^{U}(d_{jk}, d^r_{jk}, \omega)}{\cos(\omega d^r_{jk}/c)} \tag{7}$$

where d^r_{jk} is the separation distance between stations j and k in the direction of plane wave propagation and c is the best-fit plane wave speed.

Figure 8 shows the difference between 'lagged coherency' and 'plane-wave coherency' for the coherency model of Abrahamson [27] constructed by using database from earthquakes at Lotung in Taiwan in 1986. One can remark the important difference between the two aforementioned coherencies: the two coherencies have the same value for low frequencies, but at high frequencies, the lagged coherency stays constant while the plane-wave coherency keeps decreasing toward zero.

Because soil–structure interaction analyses generally assume a single plane wave, the plane wave coherency is consistent with the intended application. In other words, the 'plane wave coherency' function can be used to evaluate the standard engineering practice of modelling the wave-field by a single plane-wave. Hence, only plane-wave coherency will be analysed and presented in the following of this paper.

3.2. Statistical properties of coherencies

The statistical estimation of coherency can lead to a bias and a variance. The statistics of the (smoothed) plane-wave coherency estimate are not simple as discussed by Abrahamson [30] and Zerva [3]. It is noted that the variability of the coherency is not constant: the variability increases as $\gamma^{PW}(d_{jk}, \omega)$ decreases (the coherency is heteroscedastic). Figure 9(left) [26] presents property of plane-wave coherency. The coherency should be transformed so that it is approximately normally distributed. A $\tanh^{-1}$ transformation is often applied to the coherency to produce approximately normally distributed data [31]. That is, the $\tanh^{-1}(\gamma^{PW})$ will be approximately normally distributed about the median $\tanh^{-1}(\gamma^{PW})$ curve. Figure 9(right) shows that with this transformation the scatter of the coherency is independent of frequency (homoscedastic).

3.3. Coherency models in literature

3.3.1. Empirical coherency models. One of the most used coherency models in the USA in these last 10 years is the one developed by Abrahamson [26]. Abrahamson developed two different coherency

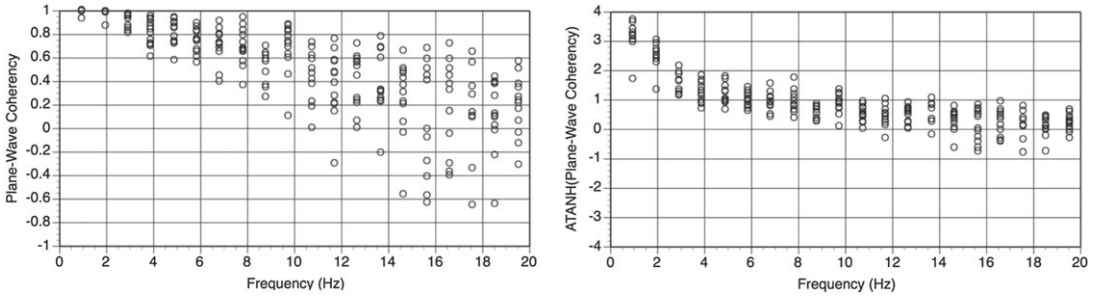

Figure 9. Dependences of variability of plane-wave coherency (left) and of transformed plane-wave coherency (right) with frequency (from [26]).

models that are corresponding to two different types of soil : soft-soil and hard rock. To do so, with the five available dense arrays (LSST, Chiba, Imperial Valley, Hollister Differential and Pinyon Flat), the author divided them into two groups on the basis of the shear-wave velocity for the top 30 m (V_{s30}). The first four dense arrays are put in the type of soft-soil because the shear-wave velocity in the sites are significantly small (V_{s30} is between 180 and 290 m/s). The last dense array (Pinyon Flat) is put in the type of hard rock site because the shear-wave velocity in the site is $V_{s30} = 1030$ m/s. The coherency model of Abrahamson is given by

$$\gamma^{PW}(d_{jk},\omega) = \left[1 + \left(\frac{\omega \cdot \tanh(a_3 \cdot d_{jk})}{2\pi \cdot f_c \cdot a_1}\right)^{n_1}\right]^{-0.5} \times \left[1 + \left(\frac{\omega \cdot \tanh(a_3 \cdot d_{jk})}{2\pi \cdot a_2}\right)^{n_2}\right]^{-0.5} \quad (8)$$

in which the parameters $a_1, a_2, a_3, f_c, n_1, n_2$ of the soft-soil sites are different from those of the hard-rock sites, and d_{jk} is the distance between two observation points j and k. To be noted that the circular frequency ω is not used in the original model of Abrahamson but it is written here to be consistent with other coherency definitions in this paper.

For the coherency model of the soft-rock sites, or hard soil sites (V_{s30} varies from 300 to 700 m/s), Abrahamson could not formulate a rigorous model because he explained in [26] that the available sites have particular topography that can influence significantly the coherency of seismic ground motions. The author mentioned that for soil–structure interaction applications on soft-rock sites, it is recommended that the average of the soil and hard-rock coherency should be used.

The models of Abrahamson have been accepted by the United States Nuclear Regulatory Commission for using in the designs of nuclear power plants. However, because these models are empirically constructed, it is not reliable to apply them into the analyses of seismic soil–structure interactions for other arbitrary sites because the models might not provide a satisfactory coherency when they are used for other sites that may have different profiles from the sites used by Abrahamson. To clarify this remark, the *in situ* coherency estimated from Argostoli dense array will be compared to the model of Abrahamson (hard-rock site) in the following of this paper.

Another empirical coherency model to be cited as one of the most widely used models in the literature might be the one of Harichandran and Vanmarcke [32]. Because the model was constructed on the basis of the notion of *lagged coherency* and appropriate only for the inter-station distances <100 m, the latter one is not used for the comparison with our analyses in this paper because we are interested only in the case of *plane-wave coherency* for the inter-station distances from 10 to 100 m.

3.3.2. Semi-empirical coherency models. Semi-empirical models are formed on the basis of analytical considerations but include parameters that require estimation from recorded data. One of the most quoted coherency models is maybe the one introduced by Luco and Wong [4] considering the propagation of shear waves in a random medium. For this model, the coherency for a pair of accelerations at two different stations with a separation distance d_{jk} is given by

$$\gamma^{PW}(d_{jk},\omega) = \exp\left[-\left(\frac{\alpha\cdot\omega\cdot d_{jk}}{V_s}\right)^2\right] \tag{9}$$

where V_s is the average shear wave velocity of the ground medium along the wave travel path, and α is the coefficient of spatial variability which can be defined by using recorded data from earthquake site.

Because α and V_s are two constant parameters, the expression of the model of Luco and Wong is often replaced by $\eta = \alpha/Vs$. Luco and Wong suggested the typical values of η in the range from 2×10^{-4} to 3×10^{-4} s/m [4].

Several studies have been reported in the literature [18, 25] to determine the value of the parameter α (or η). Until now, this parameter is still an unknown one because there is not any exact conclusion on the value of that parameter. Konakli *et al*. [18] revisited the model of Luco and Wong [4] by comparing this model with the coherency estimated from accelerograms recorded by the UPSAR array during the 2004 Parkfield earthquake. The authors concluded that the parameter η cannot be constant, but that latter one depends strongly on the station separations and weakly depends on the frequency. The parameter α (or η) and the functional form of this model will be discussed again in Section 5 when it is compared to the coherencies estimated from Argostoli database.

There are also other models proposed in literature, like the one of [1] or the one developed by [33]. They are not presented in this paper.

4. SPATIAL COHERENCY ESTIMATED FROM ARGOSTOLI DENSE ARRAY

The statistical analyses of spatial coherencies of seismic ground motions estimated from Argostoli database are presented in what follows. First of all, the spatial coherency estimated from strong motion windows is presented. For each separation distance of stations, the dispersions of all coherencies estimated from 93 earthquake events are presented to show how the coherency varies for different earthquake events. After that, we aim to investigate the coherency estimated from coda part of earthquake ground motion signals. The dependences of coherency with event number and strong motion duration are also discussed.

As described in Section (3.1.4), to evaluate the plane-wave coherency, one needs to search for the direction of plane-wave propagations and best plane wave velocity for each earthquake event. Figure 10 presents the distribution of the angle ϕ for the events used for estimating coherencies. It is reminded that the angle ϕ is evaluated by letting the coefficient of correlation ρ be equal to zero (Equation 6). Note that the found angles correspond very well to the azimuths of earthquake events presented in

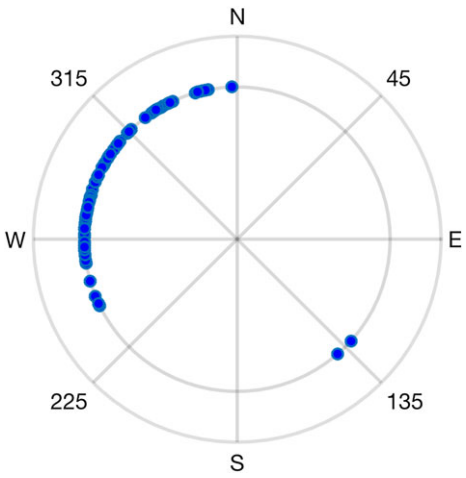

Figure 10. Distribution of angle ϕ representing the directions of plane-wave propagations. The center of circle corresponds to the station array. [Colour figure can be viewed at wileyonlinelibrary.com]

Figure 3 in which most of the earthquake sources are situated in the direction north-west of the station array.

For each event, the signals are rotated to the direction of plane-wave propagation, and the 'best-fit' plane wave velocity can be evaluated by aligning the stations to the direction of plane-wave propagation. As discussed by Abrahamson in [27], it is possible that each event or each pair of stations can give different values of 'best fit' plane wave velocity, but for the analyses of Argostoli database, it is observed that the 'best fit' plane wave velocity is approximatively constant and gives the slowness to be around 0.175 s/km. In his analyses on Lotung site in Taiwan [27], and Pinyon Flat site in the USA [26], Abrahamson also observed the constant apparent velocity of 'best-fit' plane wave propagations.

4.1. Spatial coherency estimated from strong motion windows

With the 93 earthquake events used for estimating coherencies, the strong motion windows which can be determined from 10%AI to 90%AI (Equation 2) can vary from 1 to 10 s depending on epicentral distance and magnitude of events. The length of strong motion windows increases in parallel with epicentral distances, but for most of the analysed events, the strong motion durations are around 5 s because many of the analysed events have almost the same epicentral distances (Figure 4).

The plane-wave coherencies estimated from 93 different earthquake events are presented in Figure 11. The station separations of 10, 30, 55 and 100 m for horizontal component are shown. The average of all coherencies estimated for the same station separations are also presented (the blue bold line). As discussed by Abrahamson [30] and reported in Section 3.2, the plane-wave coherencies of all events are presented in ($\tanh^{-1}$) transforms because its distribution is considered to be a normal distribution.

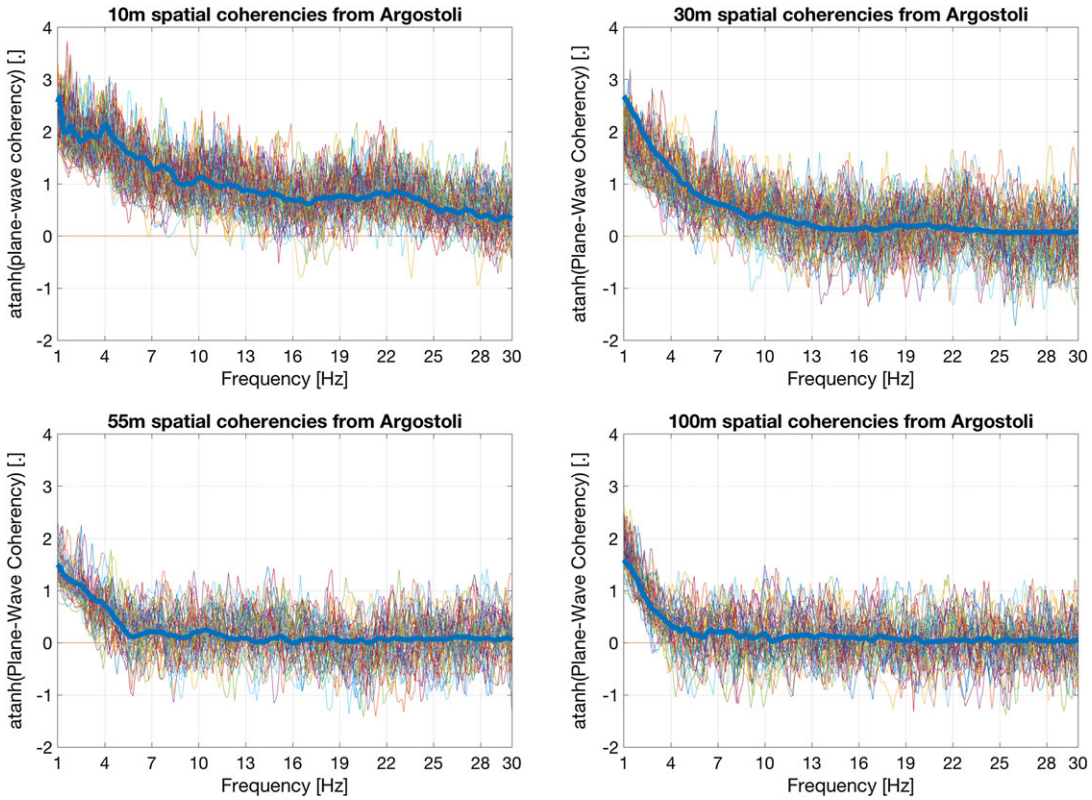

Figure 11. Dispersions of horizontal plane-wave coherences estimated from 93 events of Argostoli database for 10, 30, 55 and 100 m of separations. The blue bold line represents the average of plane-wave coherencies. [Colour figure can be viewed at wileyonlinelibrary.com]

The plane wave coherencies for vertical components are also estimated from Argostoli database. The comparisons between the averages of plane-wave coherencies estimated from horizontal component and those estimated from vertical component are shown in Figure 12. Once again, the station separations of 10, 30, 55 and 100 m are presented. For each separation distance, the difference between two plane-wave coherencies estimated from horizontal component and vertical component of signals can be remarked. However, that difference does not seem significant compared with the dispersion of all coherencies estimated for same station separations presented in Figure 11. Hence, for Argostoli database, there is not an exact conclusion about whether the coherencies of horizontal components are bigger or smaller than those of vertical components. This might be explained by the fact that the Argostoli dense array is situated on a rock site where the soil can be considered to have isotropic properties.

The residuals of plane-wave coherencies estimated from 93 different earthquake events for horizontal component are also evaluated and presented in Figure 13. The residuals presented here are simply the difference between the plane-wave coherencies of different events and the average of plane-wave coherencies presented in Figure 12. With the transform $\tanh^{-1}(Coherency)$, one can remark exactly that the variation of coherencies from different events remains approximatively constant with frequencies. From 10 to 100 m of station separations, the difference in terms of residual of coherencies is not significant although the plane-wave coherency for 100-m distance is very small compared with that of 10 m. The residuals of vertical component for station separations of 10 and 100 m are also presented in Figure 14. It can be remarked that the residuals of coherencies from vertical component are almost the same to those from horizontal components. No significant difference can be observed from those two Figures (13 and 14). The residuals presented here can also confirm the fact that the difference between the plane-wave coherencies estimated from horizontal and vertical components can be neglected.

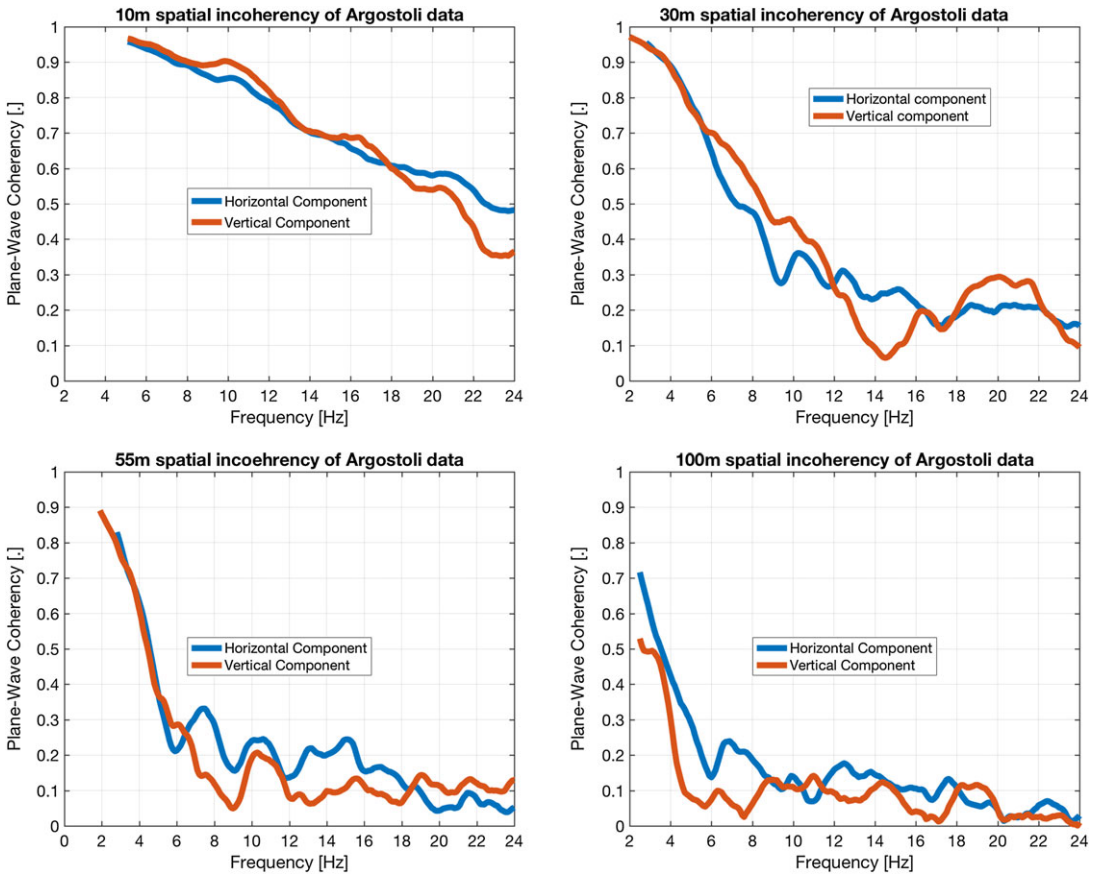

Figure 12. Spatial incoherency estimated from Argostoli database for 10, 30, 55 and 100 m of separations. [Colour figure can be viewed at wileyonlinelibrary.com]

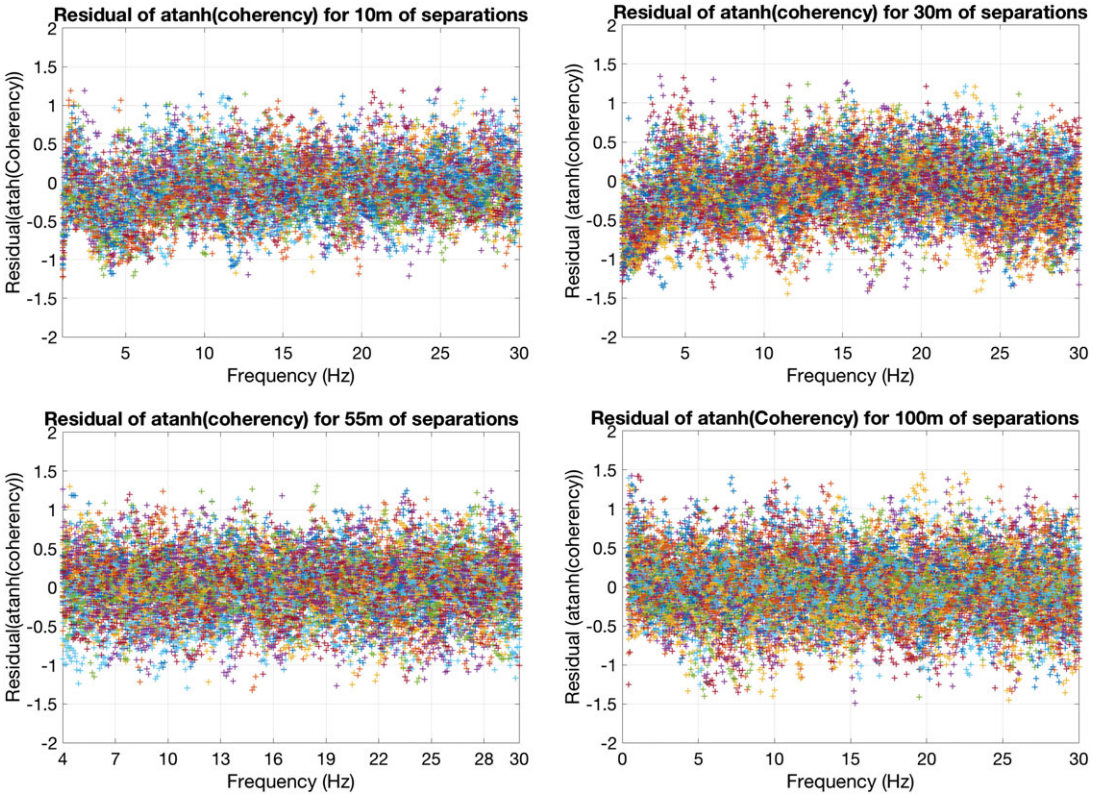

Figure 13. Residuals of $\tanh^{-1}(coherencies)$ of horizontal component from 93 earthquake events for 10m, 30m, 55m and 100m of separations. [Colour figure can be viewed at wileyonlinelibrary.com]

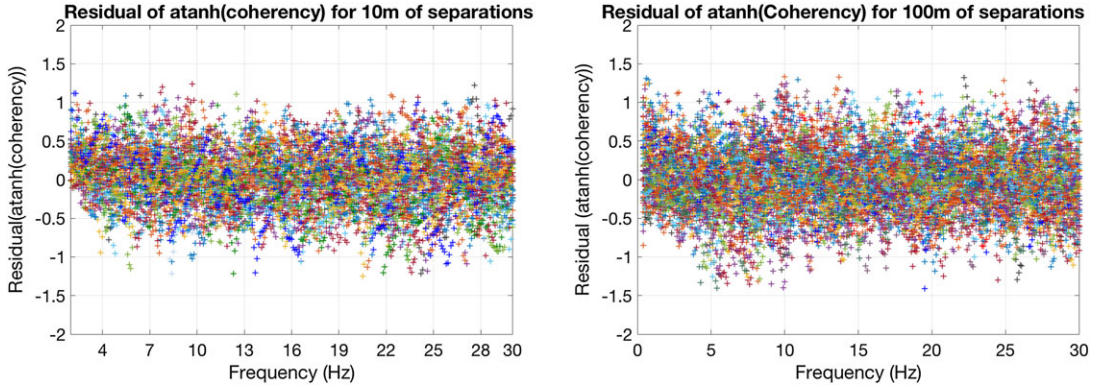

Figure 14. Residuals of $\tanh^{-1}(coherencies)$ of vertical component from 93 earthquake events for 10 and 100 m of separations. [Colour figure can be viewed at wileyonlinelibrary.com]

4.2. Spatial coherency estimated from coda of seismic signals

Another interesting point about spatial coherencies of earthquake ground motions is to investigate on the coda part of the ground motion signals. The coda part of signals refers to the last part of signals where the amplitude of the motions is significantly small compared with the strong motion window. First of all, the window of $AI \geqslant 0.9$ (Equation 2) is taken to represent the coda window of the signal (the green color part of Figure 7). The point of $AI = 0.9$ is taken to be the beginning of coda windows because it is considered to be the end of strong motion window as described in Section 4.1. But for some cases, it seems that at $AI = 0.9$, the coda window still consists of some high amplitudes

of signals that are not consistent to the definition of coda window. Hence, for our analyses, to avoid the influences of strong motions of signal on coda window, the windows of $AI \geqslant 0.97$ are considered to be coda window of signals for Argostoli database. With that definition, the length of coda windows varies from 3 to 10 s. To estimate the plane wave coherency, the directions and velocities of plane wave propagations are considered to be the same as the case of strong motion window, and the spectral densities are also smoothed with an 11-Hamming window function as the case of strong motion windows. Figure 15 presents the comparison of those two coherencies. Although it seems that the coherencies estimated from coda parts are smaller than those estimated from strong motion windows, the difference is not really significant here, and it can be considered to be in the range of standard deviation of coherencies estimated from strong motion windows (Figure 11). One can also analyse the variability of coherencies estimated from coda windows by investigating the residual of $\tanh^1(coherency(coda))$ (Figure 16). The first point to be concluded from that result by comparing with Figure 13 is that the residual of plane-wave coherencies estimated from coda window seems to be a bit smaller than that estimated from strong motion windows. This means that the variability of coherencies estimated from coda windows seems to be smaller than that estimated from strong motion windows.

These results show that with a sufficient number of earthquake events, the coda windows and the strong motion windows of signals give the same spatial coherencies of earthquake ground motions. It is interesting in terms of engineering applications because it suggests that the plane-wave coherencies of earthquake signals on rock sites can be identified from the coda parts of signals that can be more or less estimated from some feasible experiments on a given site. This remarkable conclusion should be investigated more precisely for other earthquake sites.

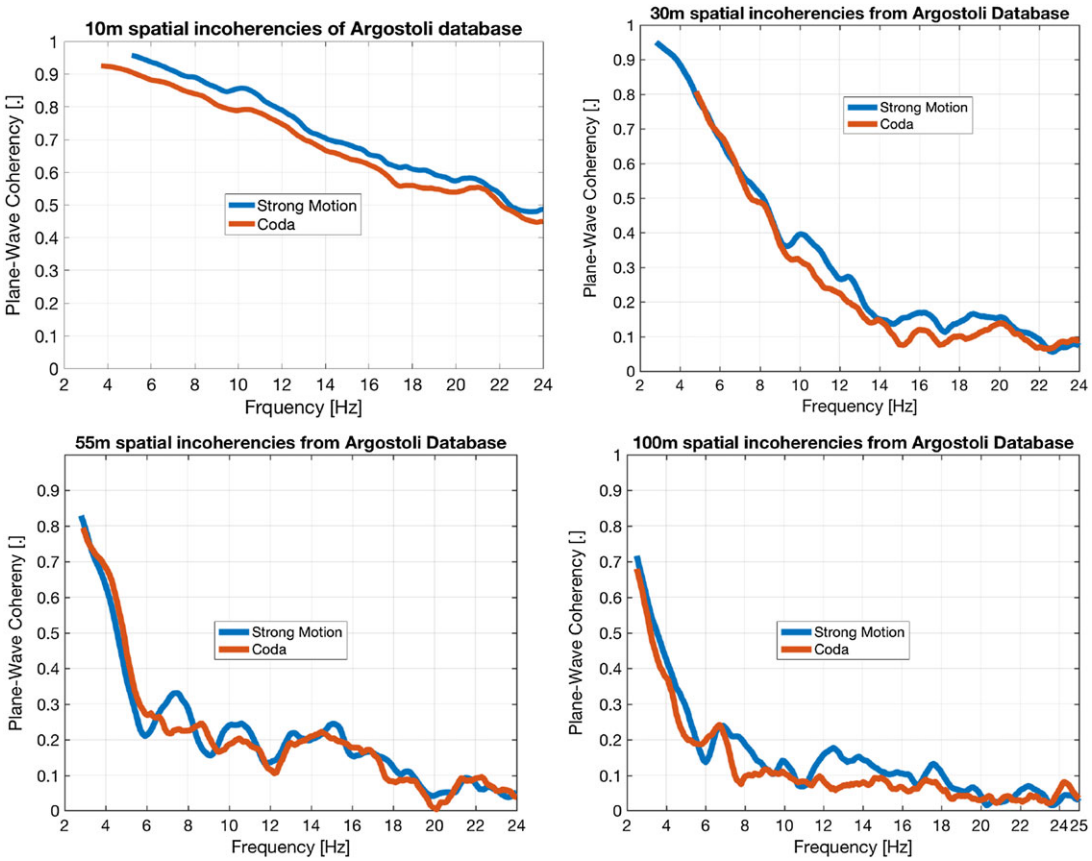

Figure 15. Comparison between coherencies estimated from strong motion windows and from coda parts of signals for 10, 30, 55 and 100 m of separations. [Colour figure can be viewed at wileyonlinelibrary.com]

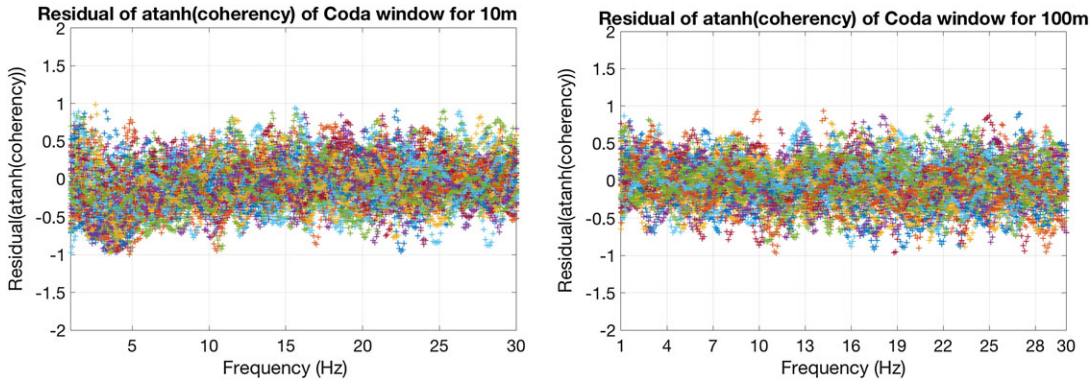

Figure 16. Residual of $tanh^{-1}(coherencies)$ estimated from coda window of ground motion signals for 10 and 100 m of station separations. [Colour figure can be viewed at wileyonlinelibrary.com]

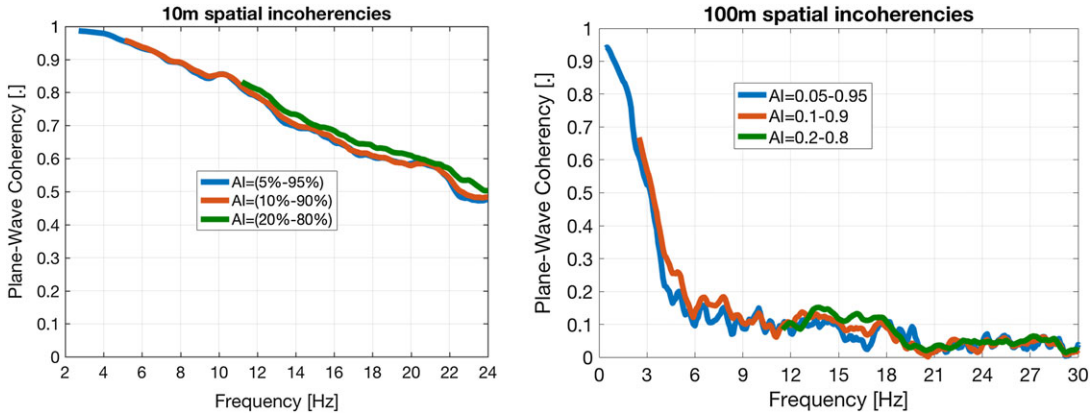

Figure 17. Comparison between coherencies estimated from different strong motion durations of signals for 10 and 100 m of separations. [Colour figure can be viewed at wileyonlinelibrary.com]

4.3. Influences of the strong motion durations on spatial coherency

As described previously, the coherencies of earthquake ground motions are estimated from strong motion windows of earthquake signals defined from Arias Intensity (Equation 2). Another analysis which should be carried out is to investigate the influence of that duration on the spatial coherencies. To do so, the comparison between the coherencies estimated from different durations of strong motions is realized and presented in Figure 17. In that figure, the station separations of 10 and 100 m are presented because they are respectively the smallest and the biggest separation distances that are analysed in our studies. Three different durations are presented: the window of $AI = 0.05 - 0.95$, the window of $AI = 0.1 - 0.9$ and the window of $AI = 0.2 - 0.8$. One can remark that the strong motion duration does not strongly influence the coherencies. This result could be expected because no difference was found between the coherencies estimated from coda parts and strong motion windows. Nevertheless, the fact of taking a short strong motion duration can lead to the loss of resolutions in frequency. It can be concluded from this analysis that the strong motion durations can be defined from $AI = 0.05$ to $AI = 0.95$ (or from $AI = 0.05$ to $AI = 0.9$) to obtain a high resolution in frequencies.

4.4. Influence of the number of earthquake events on spatial coherency

Because the coherencies of seismic ground motions presented earlier are obtained by statistical analyses from 93 different earthquake events, it is necessary to study the convergence of coherencies. Simply, it aims to understand about the sufficient number of earthquake events that can give a good estimation of coherencies. This analysis is shown in Figure 18. The averages of plane-wave coherencies estimated from 20, 30, 50 and 70 events of earthquakes are presented. The events are randomly selected

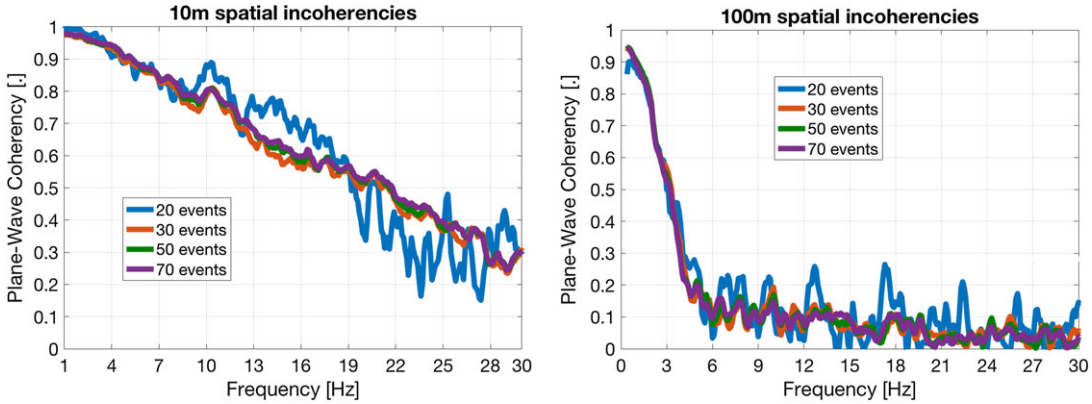

Figure 18. Comparison between coherencies estimated from different numbers of earthquake events for 10 and 100 m of separations. [Colour figure can be viewed at wileyonlinelibrary.com]

Table I. Parameters of Abrahamson model for rock site (Pinyon Flat).

Parameters	Values for rock site (Pinyon Flat)
$a1$	1.0
$a2$	40
$a3$	0.4
f_c	$27.9 - 4.82 \cdot \ln(d_{ij} + 1) + 1.24 \cdot (\ln(d_{ij} + 1) - 3.6)^2$
n_1	$3.8 - 0.04 \cdot \ln(d_{ij} + 1) + 0.0105 \cdot (\ln(d_{ij} + 1) - 3.6)^2$
n_2	16.4

for each category from the available 93 events. Once again, the station separations of 10 and 100 m are selected to illustrate the results. It is shown that for 20 earthquake events, the average of plane-wave coherencies does not converge properly yet, while for 30 events, the average of plane-wave coherencies converges and has almost the same value to the cases of 50 events and 70 events. Consequently, it is concluded that only about 30 earthquake events can already give a good estimation of coherencies. To be noted also that for the same station separations, with the dense array presented in Figure 2, we have about four or five pairs of stations. This means that for 30 earthquake events, we have around 120 realizations of coherencies. These convergence properties might be applicable only in the case of plane-wave coherencies because all the signals are rotated to the direction of plane-wave propagation. These convergence properties should also be examined for other earthquake dense arrays because it is possible that the convergence properties change from one site to another site.

5. COMPARISON BETWEEN IN SITU SPATIAL COHERENCY AND EXISTING COHERENCY MODELS

In this section, the plane-wave coherencies estimated from Argostoli database are compared with existing coherency models that are reviewed in Section 3.3: the models of Abrahamson (Equation 8) and of Luco and Wong (Equation 9). Two comparisons are presented here. For the first one, the parameters of Abrahamson model are not changed and are the same to those given by Abrahamson [26] for Pinyon Flat rock dense array. The value each parameter is listed in Table I. For the model of Luco and Wong, the parameter η was defined to be 2.5×10^{-4} s/m because this value is recommended by Luco and Wong [4]. Figure 19 illustrates the comparison. It is shown clearly that none of these two models can represent the coherencies estimated from Argostoli database if their parameters are not changed. The fact that coherencies estimated from Argostoli database are significantly smaller than coherencies of Abrahamson model (rock site) might be explained by the fact that shear-wave velocity of Argostoli site ($V_{s30} \approx 830 m/s$) is smaller than that of Pinyon Flate site ($V_{s30} \approx 1030$ m/s), which is the site used by Abrahamson for establishing his empirical model.

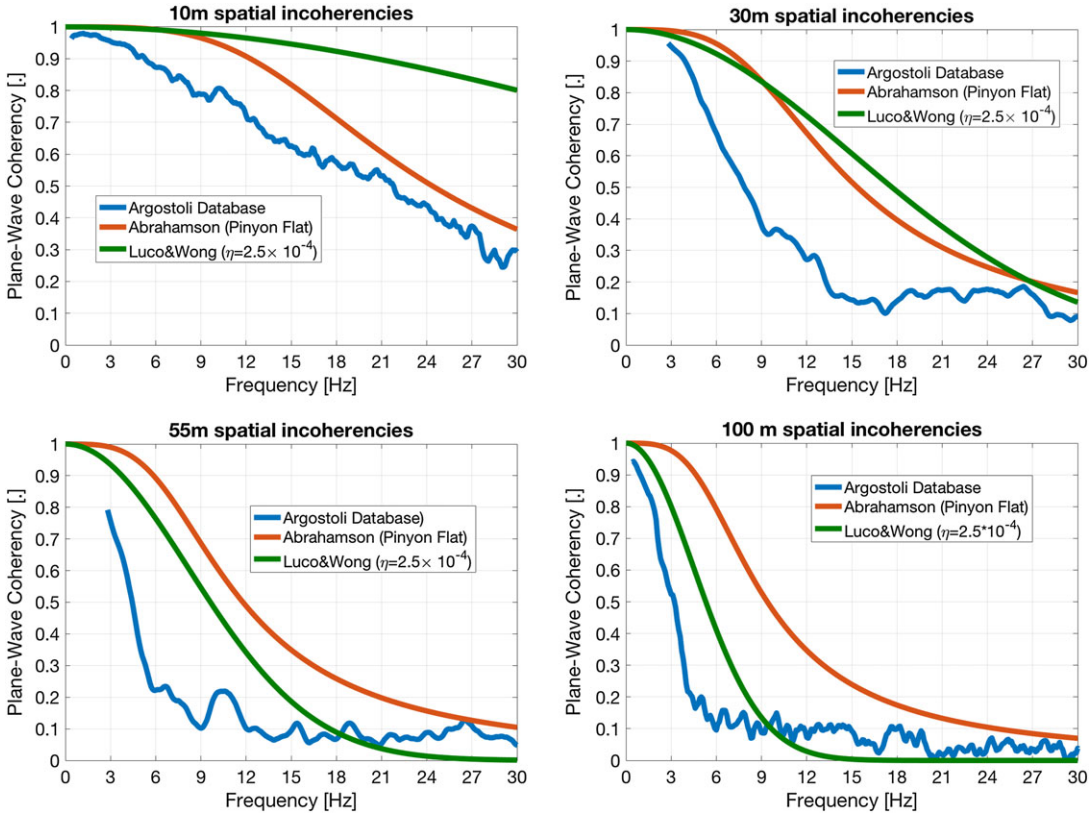

Figure 19. Comparison between coherencies estimated from Argostoli database and existing coherency models for 10, 30, 55 and 100 m of separations. [Colour figure can be viewed at wileyonlinelibrary.com]

Table II. Parameters of Abrahamson model for Argostoli dense array.

Parameters	Values fitted for Argostoli dense array
$a1$	1.0
$a2$	40
$a3$	0.4
f_c	$23.1797 - 5.1567 \cdot \ln(d_{ij} + 1) + 2.4428 \cdot (\ln(d_{ij} + 1) - 3.6)^2$
n_1	$2.8634 + 0.0579 \cdot \ln(d_{ij} + 1) - 0.2226 \cdot (\ln(d_{ij} + 1) - 3.6)^2$
n_2	16.4

For the second comparison, the parameters of Abrahamson model are modified to fit the value of coherencies estimated from Argostoli database. The parameter α of the model of Luco and Wong is also estimated to fit the model with *in situ* coherencies. By using non-linear regression curve fitting of coherencies for frequency range from 1 to 30 Hz, it is found that only the parameters f_c and $n1$ of Abrahamson model are needed to be changed to fit the model with Argostoli coherency. Other parameters stay the same to the case of Pinyon Flat database. It is remarked in these studies that the fittings performed in the transformed $\tanh^{-1}$ scale and in the original coherency scale give the same value of the defined parameters. The parameters of Abrahamson model which are fit to the Argostoli coherencies are listed in Table II. The different values of f_c for different station separations are presented in Figure 20 (left).

For the coherency model of Luco and Wong (Equation 9), as what is realized in [18], it is found that the value of α is not constant and can vary in function of distance of station pair. The values of α for different station separations are presented in Figure 20 (right). The shear-wave velocity used in this comparison is the shear-wave velocity of the top 30 m which is about 830 m/s. It should be remarked that for the small separation distance ($d = 10$ m), the coherency curve fitting is realized

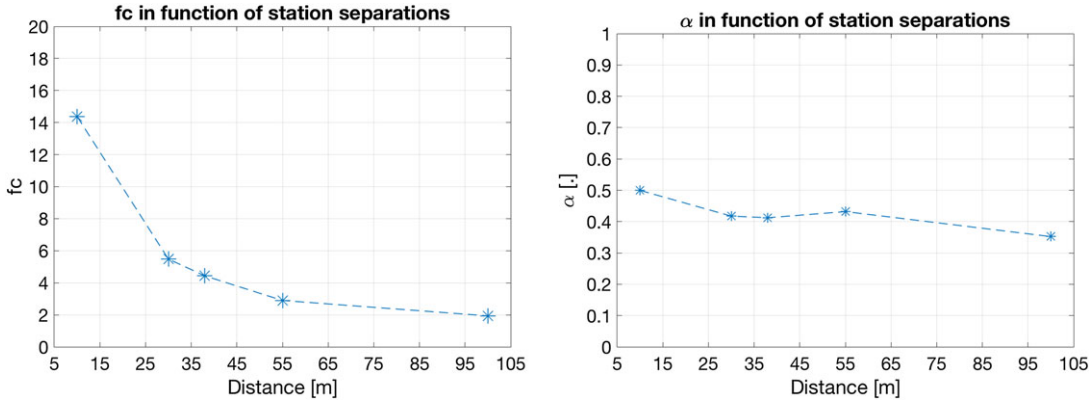

Figure 20. The values of parameters used for fitting existing coherency models with Argostoli coherencies. Left: fc in function of station separations (for Abrahamson model). Right: α in function of station separations (for the Model of Luco and Wong). [Colour figure can be viewed at wileyonlinelibrary.com]

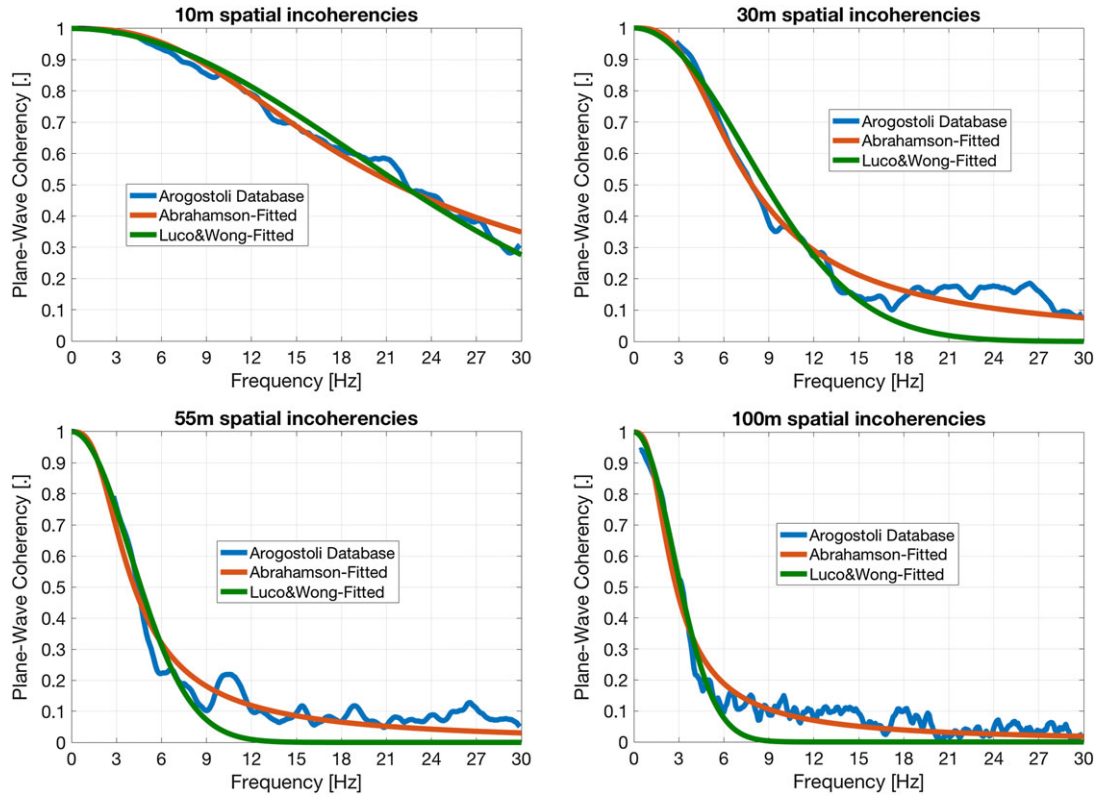

Figure 21. Comparison between coherencies estimated from Argostoli database and modified (fitted) coherency models for 10, 30, 55 and 100 m of separations. [Colour figure can be viewed at wileyonlinelibrary.com]

for the frequencies range from 1 to 30 Hz. But for larger separation distances, the coherency curve fitting does not give a good agreement for high frequencies: the frequency of curve fitting ranges from 1 to 18 Hz for 30 m of station separations, from 1 to 10 Hz for 55 m of station separations and from 1 to 6 Hz for 100 m of station separations. The fitted coherency models and Argostoli coherencies are presented in Figure 21. The author in [18] also found similar conclusions for the analysis of 2004 Parkfield earthquakes.

After these comparisons, it can be concluded that the functional form of Abrahamson model seems to be well adapted to the *in situ* coherencies, especially for high frequencies. For the model of Luco and

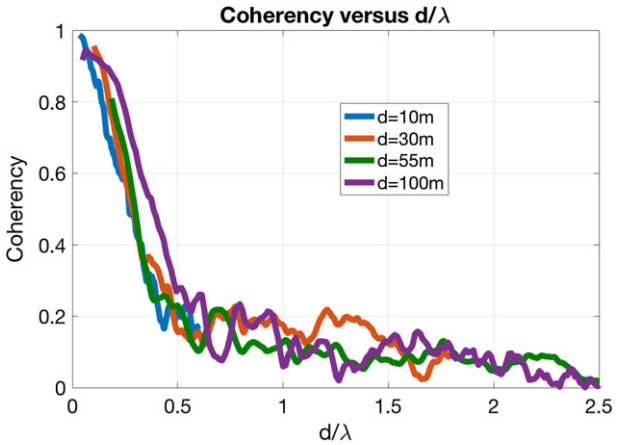

Figure 22. Coherencies in function of d/λ. [Colour figure can be viewed at wileyonlinelibrary.com]

Wong, it seems that the model tends to zero faster than experimental coherencies. Talking about the value of parameter α of Luco and Wong model, by fitting exactly the *in situ* coherencies to the model, it seems that the variation of α is more or less moderate, from which the average value $\alpha = 0.41$ could be chosen for fitting the model to the *in situ* coherencies (Figure 20–right).

If we investigate the coherencies as a function of the ratio between the station separation (d) and wavelength (λ), an interesting result can be observed as presented in Figure 22. The wavelength presented here is simply a ratio between shear-wave velocity (V_{s30}) and frequency of signals. For frequency varying from 0 Hz to 30 Hz, the value of ($1/\lambda$) can vary from 0 to 0.036 m^{-1}. For different station separations, it seems that all the coherencies are approximately the same. With this investigation, one can conclude that the functional form of the semi-empirical coherency model should be taken in function of d/λ. The functional form of the model of Luco and Wong (Equation 9) seems to be consistent with this conclusion, but we need to observe more precisely about the value of parameter α and about the power of (d/λ).

6. CONCLUSIONS

The analysis of spatial coherencies of seismic ground motions estimated from Argostoli database for small separation distances is presented. The magnitude of the analysed events varies from 2.7 to 3.6. It can be said that this analysis concerns only the relatively weak aftershocks (magnitudes smaller than 4) and cannot be generalized for the earthquake events with magnitudes higher than 4. Anyway, Abrahamson remarked in [26] that the earthquake magnitude does not influence the spatial coherency of seismic motions.

In terms of influence of signal components on coherencies, it is remarked that there is no significant difference between the coherencies estimated from horizontal component and those from vertical component. Because the coherencies are estimated from strong motion windows of earthquake signals, two other analyses are realized. Firstly, the differences between coherencies estimated from strong motion windows and those from coda parts of signals are analysed. For Argostoli database, it is shown that both parts of signals give the same coherencies. The result of this analysis is interesting in terms of engineering applications because the coherencies can be estimated by knowing only coda parts of signals. This conclusion needs to be observed on other *rock* sites. Secondly, the analyses of influences of strong motion durations are presented. Consequently, it is recommended that the coherencies should be estimated from strong motion windows that can be defined from Arias Intensity by considering the moments when $AI = 0.5$ and $AI = 0.95$ as respectively the beginning and the end of strong motion windows so that high resolutions in frequencies for coherency estimations are obtained. Regarding the convergence of coherency, the statistical analyses show that only about 30 earthquake events can already give a good estimation of spatial coherencies.

Finally, the most important analysis of these studies is to compare the coherencies estimated from Argostoli database with some existing coherency models in the literature. The coherency models that are used to be compared here are those of Abrahamson and Luco and Wong. It is shown that neither Abrahamson model nor Luco & Wong model can represent the coherencies of Argostoli database if their parameters are not modified. For small separations, it seems that Abrahamson model is comparable with coherencies of Argostoli database, but the difference becomes important for large separations. For the model of Luco and Wong, the difference is significant for small separations but becomes closer to the Argostoli coherencies for large separations. This result shows clearly that existing coherency models may provide unsatisfactory estimations of the actual site-specific coherency values.

Nevertheless, by modifying the value of some parameters, both coherency models seem to represent better the *in situ* coherencies. The most important conclusions of these analyses should be

(1) Although Abrahamson model [26] was normally used in literature to represent the coherencies of rock sites, some of its parameters should be modified by using *in situ* results before being used in soil–structure interaction analyses.
(2) For the model of Luco and Wong [4], the first conclusion from fitting with in situ coherencies is that the parameter α can vary moderately in function of station separations.
(3) The limitation of those existing coherency models encourages to investigate more precisely the functional form as well as the values of each parameter before applying them in the soil–structure interaction analyses. This also encourages to establish another coherency model that can be in function of physical and statistical properties of soil so that it can be applied for any types of soil whose statistical and physical properties are known. In this context, by presenting in situ coherencies in function of ratio between station separations and wavelength, the coherencies model should be written in function of that ratio. The work of establishing a new coherency model is currently in progress.

ACKNOWLEDGEMENTS

This work was carried out within the SINAPS@ project, which benefited from French state funding managed by the National Research Agency under program RNSR Future Investments bearing reference No. ANR-RSNR-0022-04. The seismological instrumentation used for the Argostoli rock site dense array was provided by CEA, IRSN and CEREMA. We would like to thank all people that help directly or indirectly in the organization of the post-seismic survey: Chrisostomos Andreou (TEI), Cécile Cornou (ISTerre), Marc Cushing (IRSN), Alberto Frau (CEA), Sébastien Hok (IRSN), Agis Konidaris (TEI), Philippe Langlaude (CEREMA), Aurore Laurendeau (CEA), Armand Mariscal (ISTerre), Alexandros Savvaidis (EPPO-ITSAK) and Nikolaos Theodoulidis (EPPO-ITSAK).

REFERENCES

1. DerKiureghian A. A coherency model for spatially varying ground motions. *Earthquake Engineering and Structural Dynamics* 1996; **25**:99–111.
2. Harichandran RS. *Spatial Variation of Earthquake Ground Motion, What is it, How do we Model it, and What are its Engineering Implications?*, Press of Michigan State University, East Lansing, Michigan, 1999.
3. Zerva A. *Spatial Variation of Seismic Ground Motions, Modelling and Engineering Application*, CRC Press, Boca Raton, 2009.
4. Luco JE, Wong HL. Response of a rigid foundation to a spatially random ground motion. *Soil Dynamics and Earthquake Engineering* 1986; **14**:891–908.
5. EPRI. Program on technology innovation: effects of seismic wave incoherence on foundation and building responses. *Technical Report 1013504*, EPRI, Palo Alto, CA and USDOE, Germantown, MD: 2006.
6. Ghiocel D, Ostadan F. Seismic ground motion incoherency effects on soil–structure interaction response of NPP building structure, *19th International Conference on Structural Mechanics in Reactor Technology (SMiRT19)*, Toronto, 2007; Paper #K05/4.
7. Jeremic B, Tafazzoli N, Ancheta T, Orbovic N, Blahoianu A. Seismic behavior of NPP structures subjected to realistic 3D, inclined seismic motions, in variable layered soil/rock, on surface of embedded foundations. *Nuclear Engineering and Design* 2013; **265**:85–94.

8. Zentner I, Devesa G. A methodology for soil–structure interaction analysis accounting for spatially incoherent seismic free field motion, *Proceedings of the 8th International Conference on Structural Dynamics, Eurodyn 2011*: Leuven, Belgium, 2011; 589–594.
9. Tseng W, Lilhanand K, Hamasaki D, Garcia JA, Srinivasan R. Seismic soil-structure interaction with consideration of spatial incoherence of seismic ground motions: a case study. *Nuclear Engineering and Design* 2014; **269**: 200–206.
10. Mezouer N, Afra H, Silhadi K. The effects of spatial variability ground motion on structures response, *11th European Conference on Earthquake Engineering*: Paris, 1998; 547.
11. Hong H. Arch response to correlated multiple excitations. *Soil Dynamics and Earthquake Engineering* 1993; **22**:389–404.
12. DerKiureghian A, Neuenhofer A. Response spectrum method for incoherent support motions, *10th World Conference on Earthquake Engineering*: Madrid, Spain, 1992; 4757–4762.
13. Bi K., Hao H. Numerical simulation of pounding damage to bridge structures under spatially varying ground motion. *Engineering Structures* 2013; **46**:62–76.
14. Saxena V, Deodatis G, Shinozuka M. Effect of spatial variation of earthquake ground motion on the nonlinear dynamic response of highway bridges, *12 WCEE*: New Zealand, 2000; 2227–2234.
15. Konakli K, DerKiureghian A. Extended msrs rule for seismic analysis of bridges subjected to differential support motions. *Earthquake Engineering and Structural Dynamics* 2011; **40**:1315–1335.
16. Dulinska JM. Importance of ground motion spatial variability effects on earth dam. *International Journal of Earth Sciences and Engineering* 2012February; **5**(1):1–9.
17. Zerva A. On the spatial variation of seismic ground motions and its effects on lifelines. *Engineering Structures* 1994; **16**(7):534–546.
18. Konakli K, Kiureghian AD, Dreger D. Coherency analysis of accelerograms recorded by the UPSAR array during the 2004 Parkfield earthquake. *Earthquake Engineering and Structural Dynamics* 2013; **43**:641–659.
19. Valkaniotis S, Ganas A, Papathanassiou G, Papanikolaou M. Field observations of geological effects triggered by the January–February 2014 Cephalonia (Ionian Sea, Greece) earthquakes. *Tectonophysics* 2014; **630**:150–157.
20. Theodoulidis N, Karakostas C, Lekidis V, Makra K, Margaris B, Morfidis K, Papaioannou C, Rovithis E, Salonikios T, Savvaidis. The Cephalonia, Greece, January 26 (m6.1) and February 3, 2014 (m6.0) earthquakes: near-fault ground motion and effects on soil and structures. *Bulletin of Earthquake Engineering* 2016; **14**:1–38.
21. Cushing EM, Hollender F, Guvonnet-Benaize C, Perron V, Imtiaz A, Svay A, Mariscal A, Bard PY, Cottereau R, Lopez-Caballero F, Theodoulidis N, Moiriat D, Gélis C. Close to the lair of odysseurs cyclons: Sinaps@ postseismic campaign and accelerometric network installation on cephalonia island – site effect characterization experiment, *7th International INQUA Meeting on Paleoseismology, Active Tectonics and Archeoseismology (PATA)*, Vol. 7: Crestone, Colorado, 2016. ISBN 978-0-9974355-2-8. DOI: https://www.researchgate.net/publication/303985545_INQUA_Focus_Group_on_Paleoseismology_and_Active_Tectonics_Close_to_the_lair_of_Odysseus_Cyclops_the_SINAPS_postseismic_campaign_and_accelerometric_network_installation_on_Cephalonia_island_-_Site_effe.
22. BergeThierry C, Svay A, Laurendeau A, Chartier T, Perron V, Guyonnet-Benaize C, Kishta E, Cottereau R, Lopez-Caballero F, Hollender F, Richard B, Ragueneaud F, Voldoire F, Banci F, Zentner I, Moussallam N, Lancieri M, Bard PY, Grange S, Erlicher S, Kotronis P, Le-Maoult A, Nicolas M, Regnier J, Bonilla F, Theodoulidis N. Toward an integrated seismic risk assessment for nuclear safety improving current french methodologies through the Sinaps@ research project. *Nuclear Engineering and Design* 2017 (in press).
23. Hollender F, Perron V, Imtiaz A, Svay A, Mariscal A, Bard PY, Cottereau R, Lopez-Caballero F, Cushing EM, Theodoulidis N, Moiriat D. À deux pas du repaire du cyclope d'Ulysse : la campagne post-sismique et le démarrage du réseau accélérométrique sinaps@ sur l'île de céphalonie, *Proceedings of the 9th AFPS National Meeting*: Champs-sur-Marne, 2015. DOI: https://www.researchgate.net/publication/299536865_A_deux_pas_du_repaire_du_Cyclope_d'Ulysse_la_campagne_post-sismique_et_le_demarrage_du_reseau_accelerometrique_SINAPS_sur_l'ile_de_Cephalonie_Close_to_the_lair_of_Odysseus_Cyclops_the_SINAPS_post-_sei.
24. Foti S, Lai CG, Rix G, Strobbia C. *Surface Wave Methods for Near-Surface Site Characterization*, CRC Press, Boca Raton, 2014.
25. Zerva A, Harada T. Effect of surface layer stochasticity on seismic ground motion coherence and strain estimates. *Soil Dynamics and Earthquake Engineering* 1997; **16**(7-8):445–457.
26. EPRI. Program on technology innovation: effects of spatial incoherence on seismic ground motions. *Technical Report 1015110*, EPRI, Palo Alto, CA: 2007.
27. Abrahamson N, Schneider JF, Stepp JC. Empirical spatial coherency functions for application to soil–structure interaction analyses. *Earthquake Spectra* 1991; **7**(1):1–27.
28. EPRI. Program on technology innovation: spatial coherency models for soil–structure interaction. *Technical Report 1014101*, EPRI, Palo Alto, CA, and U.S. Department of Energy, Germantown, MD: 2006.
29. Rezaeian S, DerKiureghian A. Simulation of orthogonal horizontal ground motion components for specified earthquake and site characteristics. *Earthquake Engineering and Structural Dynamics* 2011; **41**:335–353.
30. Abrahamson N. Spatial variation of earthquake ground motion for application to soil–structure interaction. *Technical Report TR-100463*, EPRI, Palo Alto, CA, 1992.
31. Enochson LD, Goodman NR. Gaussian approximations to the distributions of sample coherence. *Technical Report AFFDL-TR-65-57*, Wright-Patterson Air Force Base, Ohio, 1965.
32. Harichandran RS, Vanmarcke E. Stochastic variation of earthauqke ground motion in space and time. *Journal of Engineering Mechanics, ASCE* 1986. DOI: 10.1061/(ASCE)0733-9399(1986)112:2(154).
33. Laouami N, Labbe P. Analytical approach for evaluation of the seismic ground motion coherency function. *Soil Dynamics and Earthquake Engineering* 2001; **21**:727–733.